Smart Materials and Structures

PAPER

Large rotation FE transient analysis of piezolaminated thin-walled smart structures

To cite this article: S Q Zhang and R Schmidt 2013 *Smart Mater. Struct.* **22** 105025

Smart Mater. Struct. **22** (2013) 105025 (8pp) doi:10.1088/0964-1726/22/10/105025

Large rotation FE transient analysis of piezolaminated thin-walled smart structures

S Q Zhang[1,2] **and R Schmidt**[1]

[1] Institute of General Mechanics, RWTH Aachen University, Templergraben 64, D-52056 Aachen, Germany
[2] School of Mechanical Engineering, Northwestern Polytechnical University, 710072 Xi'an, People's Republic of China

E-mail: shunqi@iam.rwth-aachen.de and shunqi.zhang@hotmail.com

Received 30 April 2013, in final form 14 August 2013
Published 10 September 2013
Online at stacks.iop.org/SMS/22/105025

Abstract
A geometrically nonlinear large rotation shell theory is proposed for dynamic finite element (FE) analysis of piezoelectric integrated thin-walled smart structures. The large rotation theory, which has six independent kinematic parameters but expressed by five nodal degrees of freedom (DOFs), is based on first-order shear deformation (FOSD) hypothesis. The two-dimensional (2D) FE model is constructed using eight-node quadrilateral shell elements with five mechanical DOFs per node and one electrical DOF per piezoelectric material layer with linear constitutive equations. The linear and nonlinear dynamic responses are determined by the central difference algorithm (CDA) and the Newmark method. The results are compared with those obtained by simplified nonlinear theories, as well as those reported in the literature. It is shown that the present large rotation theory yields considerable improvement if the structures undergo large displacements and rotations.

1. Introduction

Due to light-weight design, thin-walled structures are increasingly implemented in many fields of technology, especially in automotive and aerospace engineering. Thin-walled structures have a number of beneficial properties, e.g. reduction of weight, less raw material, etc. However, they tend to be more unstable and sensitive to vibrations. In recent decades, thin-walled structures with integrated layers or patches of smart materials, i.e. piezoelectrics, electrostrictives, magnetostrictives, shape memory alloys, which are so-called smart structures, have been proposed for vibration control, shape control, noise and acoustic control, damage detection, and health monitoring (see [1–3] among others).

Because of the high cost of experimental investigations, theoretical modeling and dynamic analysis of smart structures are essential for their design and manufacture. One of the major problems of analysis of smart structures is how to precisely predict the dynamic behavior. Numerous papers can be found in the literature which present linear piezoelectric coupled FE models using three-dimensional (3D) elements [4–6], and 2D elements based on various hypotheses, e.g. Kirchhoff–Love plate/shell theory, Timoshenko beam theory, Mindlin–Reissner plate/shell theory, third-order shear deformation (TOSD) theory or higher-order shear deformation (HOSD) theory (see [7–11] among many others). Moreover, a higher-order layerwise laminated theory and equivalent single layer theory have been proposed and developed by Carrera and Demasi [12], and Alaimo *et al* [13] for laminated plates.

Since linear models are only applicable for structures in the range of small rotations, geometrically nonlinear effects have to be considered for structures undergoing moderate or large deflections. Recently, a large number of papers have started considering geometrical nonlinearities in FE modeling for static and dynamic analysis of thin-walled structures integrated with piezoelectric layers or patches. Von Kármán type nonlinear theories, which are the simplest geometrically nonlinear theories, are widely used in modeling of smart structures. Panda and Ray [14] developed a von Kármán type nonlinear FE model, which is based on the FOSD hypothesis, for static analysis of smart structures. For dynamic analysis, a number of papers that can be found in the literature developed FE models using von Kármán type nonlinear theories based on various hypotheses, e.g. classical plate theory [15, 16], FOSD hypothesis [17, 18], and TOSD or HOSD hypotheses [19, 20]. Compared to von Kármán type nonlinearity, moderate rotation theory considers more nonlinear effects, which was first proposed by Librescu and Schmidt [21], and Schmidt and Reddy [22]. Later, the theory was further developed and implemented by Palmerio *et al* [23], Kreja *et al* [24], and Lentzen *et al* [25–27] for both static and dynamic analysis of composite or smart structures. Adding more nonlinear strain–displacement relations results in a fully geometrically nonlinear theory which was implemented by Chattopadhyay *et al* [28] and Ghoshal *et al* [29] based on improved layerwise theory for dynamic analysis of smart composite structures with consideration of delamination effect. Apart from 2D FE models, Yi *et al* [30] developed a 3D nonlinear FE model for transient analysis of a smart beam, a plate and a shell. Furthermore, Chróscielewski *et al* [31, 32] developed a one-dimensional (1D) FE model using fully nonlinear large rotation theory for shape and vibration control of curved beam-type structures.

In some applications, von Kármán type nonlinear theory and moderate rotation theory are precise enough to predict the transient response of smart structures. But for those undergoing large deformation, large rotation theories have to be considered, rather than simplified nonlinear shell theories. In recent decades, some authors considered fully geometrically nonlinear theories with arbitrary rotations, which are called large rotation theories or finite rotation theories. Most of these were applied to laminated structures made of isotropic or orthotropic materials for static benchmark problems (see [33–35, 27] among many others). Following the approach given by Kreja and Schmidt [35] for fully geometrically nonlinear static and stability analysis of composite structures with large rotations, this paper will develop a large rotation shell theory with six independent kinematic parameters, but expressed by five nodal DOFs, for dynamic analysis of piezoelectric coupled thin-walled smart structures based on the FOSD hypothesis. A nonlinear dynamic FE model is derived by Hamilton's principle and the FE method using eight-node shell elements with five mechanical DOFs per node and one electrical DOF per piezoelectric material layer. Additionally, the results obtained by the proposed large rotation theory are compared with those obtained by other simplified nonlinear theories, as well as those reported in [30, 25].

2. Strain field

Large rotation theory is the most accurate one among all nonlinear shell theories, since fully geometrically nonlinear strain terms and arbitrary finite rotations are considered in the theory. In this paper, a dynamic large rotation theory with six independent kinematic parameters that are expressed by five nodal DOFs, abbreviated as LRT56 [35], is developed based on the FOSD hypothesis for smart structures. According to the geometry relations, the components of the displacement vector $\mathbf{u}$ for an arbitrary point in the shell space at a distance Θ^3 from the mid-surface are given as

$$\begin{aligned} v_\alpha(\Theta^1,\Theta^2,\Theta^3) &= \overset{0}{v}_\alpha(\Theta^1,\Theta^2) + \Theta^3\overset{1}{v}_\alpha(\Theta^1,\Theta^2) \\ v_3(\Theta^1,\Theta^2,\Theta^3) &= \overset{0}{v}_3(\Theta^1,\Theta^2) + \Theta^3\overset{1}{v}_3(\Theta^1,\Theta^2) \end{aligned} \tag{1}$$

where $\overset{0}{v}_i$ $(i = 1\text{–}3)$ are the covariant components of the mid-surface displacement vector $\overset{0}{\mathbf{u}}$, and $\overset{1}{v}_i$ the components of the shell director rotation vector $\overset{1}{\mathbf{u}} = \bar{\mathbf{a}}_3 - \mathbf{n}$. Here $\mathbf{n}$ is a unit normal vector in the undeformed configuration and $\bar{\mathbf{a}}_3$ denotes the covariant base vector in the direction of the parameter line Θ^3 in the deformed configuration. Equation (1) can be re-written in matrix form as

$$\mathbf{u} = \mathbf{Z}_\mathrm{u}\mathbf{v} \tag{2}$$

in which $\mathbf{v}$ contains the six kinematic parameters, and $\mathbf{Z}_\mathrm{u}$ is a matrix of Θ^3.

The Green–Lagrange strain tensors of the in-plane terms, the transverse shear terms and the transverse normal term based on the FOSD hypothesis are expressed as (see [36])

$$\varepsilon_{\alpha\beta} = \overset{0}{\varepsilon}_{\alpha\beta} + \Theta^3\overset{1}{\varepsilon}_{\alpha\beta} + (\Theta^3)^2\overset{2}{\varepsilon}_{\alpha\beta} \tag{3}$$

$$\varepsilon_{\alpha 3} = \overset{0}{\varepsilon}_{\alpha 3} + \Theta^3\overset{1}{\varepsilon}_{\alpha 3} \tag{4}$$

$$\varepsilon_{33} = \overset{0}{\varepsilon}_{33}. \tag{5}$$

Using the assumption of an inextensible shell director, the transverse normal strain will be $\overset{0}{\varepsilon}_{33} = 0$, which implies $\bar{\mathbf{a}}_3 \cdot \bar{\mathbf{a}}_3 = 1$. This constraint will lead to $\bar{\mathbf{a}}_{3,\alpha} \cdot \bar{\mathbf{a}}_3 = 0$, meaning that $\overset{1}{\varepsilon}_{\alpha 3} = 0$ as well. The components of the strain tensors in equations (3)–(4) can be expressed in terms of six parameters as

$$2\overset{0}{\varepsilon}_{\alpha\beta} = \overset{0}{\varphi}_{\alpha\beta} + \overset{0}{\varphi}_{\beta\alpha} + \underline{\overset{0}{\varphi}_{3\alpha}\overset{0}{\varphi}_{3\beta}} + \underline{\underline{\overset{0}{\varphi}{}^{\delta}_{\alpha}\overset{0}{\varphi}_{\delta\beta}}} \tag{6}$$

$$\begin{aligned} 2\overset{1}{\varepsilon}_{\alpha\beta} &= \overset{1}{\varphi}_{\alpha\beta} - b^\lambda_\beta\overset{0}{\varphi}_{\lambda\alpha} + \overset{1}{\varphi}_{\beta\alpha} - b^\delta_\alpha\overset{0}{\varphi}_{\delta\beta} \\ &\quad + \underline{\overset{0}{\varphi}_{3\alpha}\overset{1}{\varphi}_{3\beta} + \overset{1}{\varphi}_{3\alpha}\overset{0}{\varphi}_{3\beta}} + \underline{\underline{\overset{0}{\varphi}{}^{\delta}_{\alpha}\overset{1}{\varphi}_{\delta\beta} + \overset{1}{\varphi}{}^{\delta}_{\alpha}\overset{0}{\varphi}_{\delta\beta}}} \end{aligned} \tag{7}$$

$$2\overset{2}{\varepsilon}_{\alpha\beta} = -b^\lambda_\beta\overset{1}{\varphi}_{\lambda\alpha} - b^\delta_\alpha\overset{1}{\varphi}_{\delta\beta} + \underline{\overset{1}{\varphi}_{3\alpha}\overset{1}{\varphi}_{3\beta}} + \underline{\underline{\overset{1}{\varphi}{}^{\delta}_{\alpha}\overset{1}{\varphi}_{\delta\beta}}} \tag{8}$$

$$2\overset{0}{\varepsilon}_{\alpha 3} = \overset{1}{v}_\alpha + \overset{0}{\varphi}_{3\alpha} + \underline{\overset{0}{\varphi}{}^{\delta}_{\alpha}\overset{1}{v}_\delta} + \underline{\underline{\overset{0}{\varphi}_{3\alpha}\overset{1}{v}_3}} \tag{9}$$

with the abbreviations $\overset{n}{\varphi}_{\lambda\alpha}$, $\overset{n}{\varphi}_{3\alpha}$ and $\overset{n}{v}_{\lambda|\alpha}$ defined as:

$$\overset{n}{\varphi}_{\lambda\alpha} = \overset{n}{v}_{\lambda|\alpha} - b_{\lambda\alpha}\overset{n}{v}_3 \tag{10}$$

$$\overset{n}{\varphi}_{3\alpha} = \overset{n}{v}_{3,\alpha} + b^\delta_\alpha\overset{n}{v}_\delta \tag{11}$$

$$\overset{n}{v}_{\lambda|\alpha} = \overset{n}{v}_{\lambda,\alpha} - \Gamma^\delta_{\lambda\alpha}\overset{n}{v}_\delta \tag{12}$$

in which $b_{\lambda\alpha}$ and b^λ_α are the covariant and mixed components of the curvature tensor, and $\Gamma^\delta_{\lambda\alpha}$ denote the Christoffel symbols of the second kind. Furthermore, $\square_{|\alpha}$ and $\square_{,\alpha}$ represent the covariant derivative and spatial derivative with respect to the coordinate axis Θ^{α}. The Greek indices vary from 1 to 2 and the overhead letter n represents 0 or 1.

Neglecting *a priori* the sixth parameter $\overset{1}{v}_3$ is permitted only for small and moderate rotations. In the case where full geometrical nonlinearities are considered, however, this would yield a theory abbreviated as LRT5 [35, 37]. Dropping the strain terms marked by double lines and assuming $\overset{1}{v}_3 = 0$ yields the moderate rotation theory with five parameters (denoted as MRT5), which was first proposed by Librescu and Schmidt [21]. Further dropping the terms marked by both single and double lines leads to the linear shell theory. Retaining the nonlinear strain–displacement relations only with the squares and products of the derivative of the transverse deflection yields the refined von Kármán type nonlinear shell theory (abbreviated as RVK5) [35, 37].

3. Finite element implementation

3.1. Constitutive equations

In this paper, linear piezoelectric coupled constitutive equations are employed. These are given by

$$\boldsymbol{\sigma} = \mathbf{c}\boldsymbol{\varepsilon} - \mathbf{e}^{\mathrm{T}}\mathbf{E} \tag{13}$$

$$\mathbf{D} = \mathbf{e}\boldsymbol{\varepsilon} + \boldsymbol{\epsilon}\mathbf{E} \tag{14}$$

where $\boldsymbol{\sigma}$, $\boldsymbol{\varepsilon}$, $\mathbf{D}$ and $\mathbf{E}$ denote the stress vector, the strain vector, the electric displacement vector and the electric field vector, respectively. Additionally, $\mathbf{c}$ denotes the elasticity constant matrix, $\mathbf{d}$ and $\mathbf{e}$ are the piezoelectric constant matrices with the relation $\mathbf{e} = \mathbf{dc}$, and $\boldsymbol{\epsilon}$ denotes the dielectric constant matrix. The electric field intensity is assumed to be constant through the thickness of the piezoelectric material layers and defined as negative gradient of the electric potential $\boldsymbol{\phi}$ (see e.g. [15, 26, 19])

$$\mathbf{E} = -\nabla\boldsymbol{\phi} = \mathbf{B}_{\phi}\boldsymbol{\phi}. \tag{15}$$

3.2. Rotational displacement

As previously mentioned, in LRT56 the six kinematic parameters are expressed by five nodal DOFs: three translational DOFs (u, v and w) and two rotational DOFs (φ_1 and φ_2) are defined. The physical quantities of the generalized rotational displacements $\hat{\overset{1}{v}}_i$ are expressed by two rotations φ_1 and φ_2 about Θ^2 and Θ^1-axis respectively using Euler angles [35] as

$$\begin{aligned}
\hat{\overset{1}{v}}_1 &= |\mathbf{a}^1|\overset{1}{v}_1 = \sin(\varphi_1)\cos(\varphi_2) \\
\hat{\overset{1}{v}}_2 &= |\mathbf{a}^2|\overset{1}{v}_2 = \sin(\varphi_2) \\
\hat{\overset{1}{v}}_3 &= |\mathbf{a}^3|\overset{1}{v}_3 = \cos(\varphi_1)\cos(\varphi_2) - 1.
\end{aligned} \tag{16}$$

In the linear or simplified nonlinear theories, small or moderate rotations are respectively assumed in structures, which leads to $\sin(\varphi_\alpha) = \varphi_\alpha$ and $\cos(\varphi_\alpha) = 1$. Therefore, equation (16) for simplified nonlinear shell theories reads

$$\hat{\overset{1}{v}}_1 = \varphi_1, \qquad \hat{\overset{1}{v}}_2 = \varphi_2, \qquad \hat{\overset{1}{v}}_3 = 0. \tag{17}$$

4. Dynamic equations

4.1. Total Lagrangian formulation

The Green–Lagrange strain tensor in equations (3)–(4) can be re-written in matrix form as

$$\boldsymbol{\varepsilon} = \mathbf{H}_1\mathbf{S} \tag{18}$$

in which $\mathbf{S}$ is the resultant strain vector, and $\mathbf{H}_1$ is the matrix of Θ^3. The physical strain vector $\hat{\boldsymbol{\varepsilon}}$ is obtained by normalization as

$$\hat{\boldsymbol{\varepsilon}} = \mathbf{K}_{\mathrm{e}}\boldsymbol{\varepsilon} = \mathbf{K}_{\mathrm{en}}\mathbf{K}_{\mathrm{et}}\boldsymbol{\varepsilon}. \tag{19}$$

Here, the diagonal matrix $\mathbf{K}_{\mathrm{e}}$ produced by normalization is a function of $(\Theta^1, \Theta^2, \Theta^3)$, which can be decomposed into $\mathbf{K}_{\mathrm{en}}$ containing Θ^3 and $\mathbf{K}_{\mathrm{et}}$ depending on Θ^1 and Θ^2. The components of $\mathbf{K}_{\mathrm{et}}$ can be integrated into the resultant strain vector generating the physical resultant strain vector $\hat{\mathbf{S}}$ as

$$\mathbf{K}_{\mathrm{et}}\boldsymbol{\varepsilon} = \mathbf{K}_{\mathrm{et}}\mathbf{H}_1\mathbf{S} = \mathbf{H}_1\mathbf{N}_{\mathrm{ms}}\mathbf{S} = \mathbf{H}_1\hat{\mathbf{S}}. \tag{20}$$

In order to apply the total Lagrangian method, three configurations are considered: the initial configuration ^{0}C, referring to the undeformed configuration; the current configuration ^{1}C, referring to the deformed configuration; and the searched configuration ^{2}C, which is a virtual configuration. The configurations are characterized by left superscripts 0, 1 and 2, and the reference configurations are denoted by left subscripts. The physical resultant strain vector in configuration ^{m}C referred to the undeformed configuration can be expressed as

$${}^m_0\hat{\mathbf{S}} = \mathbf{N}_{\mathrm{ms}}(\mathbf{A}_0 + \tfrac{1}{2}\mathbf{A}_{\mathrm{n}}({}^m_0\underset{\sim}{\boldsymbol{\theta}})){}^m_0\boldsymbol{\theta}. \tag{21}$$

Here, $\mathbf{A}_0$ and $\mathbf{A}_{\mathrm{n}}({}^m_0\underset{\sim}{\boldsymbol{\theta}})$ are the linear and nonlinear strain–displacement matrices, respectively. The increment and variation of the physical resultant strain vector can be expressed by a linear part $\mathbf{B}_{\mathrm{l}}$ and a nonlinear part $\mathbf{B}_{\mathrm{nl}}$ as

$$\Delta\hat{\mathbf{S}} = \big(\mathbf{B}_{\mathrm{l}} + \mathbf{B}_{\mathrm{nl}}\big)\Delta\mathbf{q} \tag{22}$$

$${}^2_0\delta\hat{\mathbf{S}} = \big(\mathbf{B}_{\mathrm{l}} + 2\,\mathbf{B}_{\mathrm{nl}}\big)\delta\Delta\mathbf{q} \tag{23}$$

with

$$\mathbf{B}_{\mathrm{l}} = \mathbf{N}_{\mathrm{ms}}\Big(\mathbf{A}_0 + \mathbf{A}_{\mathrm{n}}({}^1_0\underset{\sim}{\boldsymbol{\theta}})\Big)\mathbf{G}_{\mathrm{t}}\mathbf{N}_{\mathrm{t}} \tag{24}$$

$$\mathbf{B}_{\mathrm{nl}} = \tfrac{1}{2}\mathbf{N}_{\mathrm{ms}}\mathbf{A}_{\mathrm{n}}(\Delta\underset{\sim}{\boldsymbol{\theta}})\mathbf{G}_{\mathrm{t}}\mathbf{N}_{\mathrm{t}} \tag{25}$$

where the matrix $\mathbf{G}_{\mathrm{t}}$ is obtained by normalization and linearizion, $\mathbf{N}_{\mathrm{t}}$ is the matrix of the shape functions, Δ represents the incremental operator, and δ is the variational operator. Furthermore, the vector $\boldsymbol{\theta}$ is defined as

$$\boldsymbol{\theta} = \left\{\overset{0}{v}_{1,1}\ \overset{0}{v}_{1,2}\ \overset{0}{v}_{2,1}\ \cdots\ \overset{1}{v}_{3,2}\ \overset{0}{v}_1\ \overset{0}{v}_2\ \cdots\ \overset{1}{v}_3\right\}. \tag{26}$$

4.2. Equations of motion

The equations of motion can be built by using Hamilton's principle, which is given by

$$\delta \int_{t_1}^{t_2} ({}^{2}_{0}T - {}^{2}_{0}W_i + {}^{2}_{0}W_e)\,\mathrm{d}t = 0. \tag{27}$$

Here the virtual work of the inertia forces ${}^{2}_{0}T$, the internal virtual work ${}^{2}_{0}W_i$ and the external virtual work ${}^{2}_{0}W_e$ are respectively obtained as

$${}^{2}_{0}\delta T = -\int_{\Omega} {}^{2}_{0}\delta\hat{\mathbf{v}}^{\mathrm{T}}\mathbf{H}_{\mathrm{u}}{}^{2}_{0}\ddot{\mathbf{v}}\,\mathrm{d}\Omega \tag{28}$$

$$\begin{aligned}{}^{2}_{0}\delta W_i = &\int_{\Omega} {}^{2}_{0}\delta\hat{\mathbf{S}}^{\mathrm{T}}\mathbf{H}_{\mathrm{c}}{}^{2}_{0}\hat{\mathbf{S}}\,\mathrm{d}\Omega + \int_{\Omega} {}^{2}_{0}\delta\hat{\mathbf{S}}^{\mathrm{T}}\mathbf{H}_{\mathrm{e}}^{\mathrm{T}}{}^{2}_{0}\mathbf{E}\,\mathrm{d}\Omega \\ &+ \int_{\Omega} {}^{2}_{0}\delta\mathbf{E}^{\mathrm{T}}\mathbf{H}_{\mathrm{e}}{}^{2}_{0}\hat{\mathbf{S}}\,\mathrm{d}\Omega + \int_{\Omega} {}^{2}_{0}\delta\mathbf{E}^{\mathrm{T}}\mathbf{H}_{\mathrm{g}}{}^{2}_{0}\mathbf{E}\,\mathrm{d}\Omega \end{aligned} \tag{29}$$

$$\begin{aligned}{}^{2}_{0}\delta W_e = &\int_{V} {}^{2}_{0}\delta\hat{\mathbf{u}}^{\mathrm{T}}\mathbf{f}_{\mathrm{b}}\,\mathrm{dV} + \int_{\Omega} {}^{2}_{0}\delta\hat{\mathbf{u}}^{\mathrm{T}}\mathbf{f}_{\mathrm{s}}\,\mathrm{d}\Omega + {}^{2}_{0}\delta\hat{\mathbf{u}}^{\mathrm{T}}\mathbf{f}_{\mathrm{c}} \\ &- \int_{\Omega} {}^{2}_{0}\delta\boldsymbol{\phi}^{\mathrm{T}}\boldsymbol{\varrho}\,\mathrm{d}\Omega - {}^{2}_{0}\delta\boldsymbol{\phi}^{\mathrm{T}}\mathbf{Q}_{\mathrm{c}} \end{aligned} \tag{30}$$

with

$$\mathbf{H}_{\mathrm{u}} = \int_h \rho\mathbf{Z}_{\mathrm{u}}^{T}\mathbf{Z}_{\mathrm{u}}\mu\,\mathrm{d}\Theta^3 \tag{31}$$

$$\mathbf{H}_{\mathrm{c}} = \int_h \mathbf{H}_1^{\mathrm{T}}\mathbf{K}_{\mathrm{en}}^{\mathrm{T}}\mathbf{c}\mathbf{K}_{\mathrm{en}}\mathbf{H}_1\mu\,\mathrm{d}\Theta^3 \tag{32}$$

$$\mathbf{H}_{\mathrm{e}} = -\int_h \mathbf{e}\mathbf{K}_{\mathrm{en}}\mathbf{H}_1\mu\,\mathrm{d}\Theta^3 \tag{33}$$

$$\mathbf{H}_{\mathrm{g}} = -\int_h \boldsymbol{\epsilon}\mu\,\mathrm{d}\Theta^3 \tag{34}$$

where ρ is the density, and μ the determinant of the shifter tensor. Additionally, $\mathbf{f}_{\mathrm{b}}, \mathbf{f}_{\mathrm{s}}$ and $\mathbf{f}_{\mathrm{c}}$ represent the vectors of body, surface and concentrated forces, and $\boldsymbol{\varrho}$ and $\mathbf{Q}_{\mathrm{c}}$ the surface and concentrated charges, respectively. Substituting equations (28)–(30) into (27) yields the equations of motion and the sensor equations as

$${}^{1}\mathbf{M}_{\mathrm{uu}}{}^{2}_{0}\ddot{\mathbf{q}} + {}^{1}\bar{\mathbf{K}}_{\mathrm{uu}}\Delta\mathbf{q} + {}^{1}\mathbf{K}_{\mathrm{u}\phi}\Delta\phi_a = \mathbf{F}_{\mathrm{ue}} - {}^{1}\mathbf{F}_{\mathrm{ui}} \tag{35}$$

$${}^{1}\mathbf{K}_{\phi\mathrm{u}}\Delta\mathbf{q} + {}^{1}\mathbf{K}_{\phi\phi}\Delta\phi_s = \mathbf{G}_{\phi\mathrm{e}} - {}^{1}\mathbf{G}_{\phi\mathrm{i}}. \tag{36}$$

Here ${}^{1}\mathbf{M}_{\mathrm{uu}}$ represents the mass matrix, ${}^{1}\bar{\mathbf{K}}_{\mathrm{uu}}$ the total stiffness matrix containing linear and nonlinear effects, ${}^{1}\mathbf{K}_{\mathrm{u}\phi}$ the piezoelectric coupled stiffness matrix, ${}^{1}\mathbf{K}_{\phi\mathrm{u}}$ the coupled capacity matrix, and ${}^{1}\mathbf{K}_{\phi\phi}$ the piezoelectric capacity matrix. In the above equations, $\mathbf{F}_{\mathrm{ue}}$ and $\mathbf{G}_{\phi\mathrm{e}}$ denote the external force and charge vectors, while ${}^{1}\mathbf{F}_{\mathrm{ui}}$ and ${}^{1}\mathbf{G}_{\phi\mathrm{i}}$ are the in-balance force and charge vectors, respectively. Additionally, $\mathbf{q}$, $\ddot{\mathbf{q}}$ are the nodal displacement and acceleration vectors, while $\boldsymbol{\phi}_{\mathrm{a}}$ denotes the voltage vector applied on actuators and $\boldsymbol{\phi}_{\mathrm{s}}$ is the vector of sensor output voltage.

5. Numerical applications

In order to verify the present nonlinear FE method, two numerical applications have been investigated, namely a cantilevered beam and a fully clamped cylindrical shell, which were first calculated by Yi *et al* [30], and later by Lentzen and Schmidt [25]. The material properties of the piezoelectric patches bonded on the master structures are $E = 67$ GPa, $\nu = 0.33$, $\rho = 7800$ kg m^{-3}, $d_{31} = d_{32} = -1.7119\times10^{-10}$ C N^{-1}, and $\epsilon_{33} = 2.03\times10^{-8}$ F m^{-1}. Here the piezoelectric coupling coefficients d_{31} and d_{32} are different from those in [30], but the same as those in [25, 27]. The piezoelectric potential of the bonded surface is $\boldsymbol{\phi} = \mathbf{0}$, while at the upper surface of the PZT patch the physical equipotential condition is enforced. An eight-node piezoelectric coupled shell element with five mechanical DOFs per node and one electrical DOF per piezoelectric layer, the element type of which is abbreviated as SH851URI for uniformly reduced integration and SH851FI for full integration, are employed in this paper.

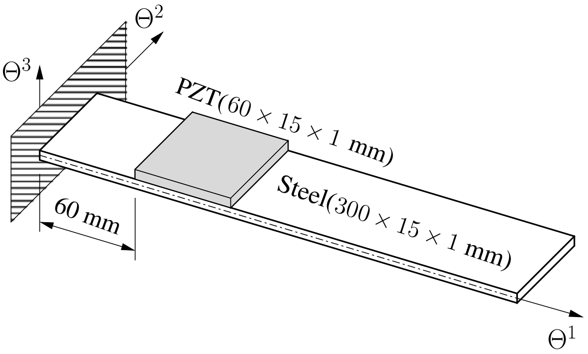

Figure 1. A cantilevered beam bonded with a piezoelectric patch.

5.1. Cantilevered beam

The first example is a cantilevered beam bonded with a piezoelectric patch, presented in figure 1. The material properties of the master structure are $E = 197$ GPa, $\nu = 0.33$, and $\rho = 7900$ kg m^{-3}. Two meshes of 5×1 and 10×1 eight-node elements are used in the following calculations, respectively. A concentrated step force of 10 N is applied on the tip point of the free end. The linear dynamic response is calculated by the Newmark method with a time step of 1×10^{-3} s. The nonlinear dynamic response using the SH851FI elements is determined by the CDA method with a time step of 1×10^{-7} s, while the Newmark method with a time step of 5×10^{-6} s is applied for the model using SH851URI elements. The tip displacement and sensor voltage transient responses obtained by various nonlinear theories using SH851URI elements are presented in figures 2 and 3, respectively. It can be seen from figure 2 that LRT56 yields a stiffer response than RVK5, but a softer one than MRT5 and LRT5. These simplified nonlinear theories fail because in this problem really large rotations occur. A deeper investigation of the structure shows that under a quasi-statically applied tip force 10 N, the structure undergoes maximum rotations of more than 50°. Furthermore, the static deflections predicted by LRT56 are larger than those by MRT5 and LRT5.

The next group of figures shows the transient responses obtained by LRT56 theory using both SH851URI and

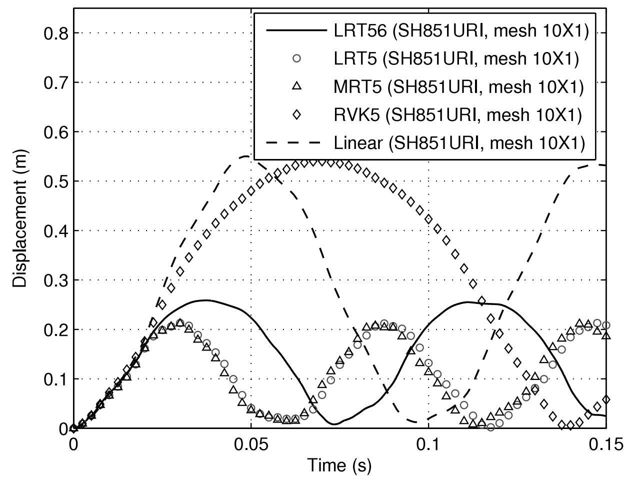

Figure 2. Tip displacement of the cantilevered beam using various theories.

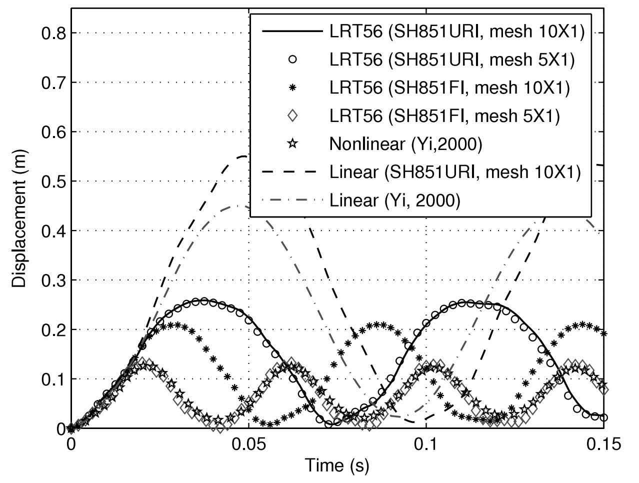

Figure 4. Tip displacement of the cantilevered beam using LRT56 theory.

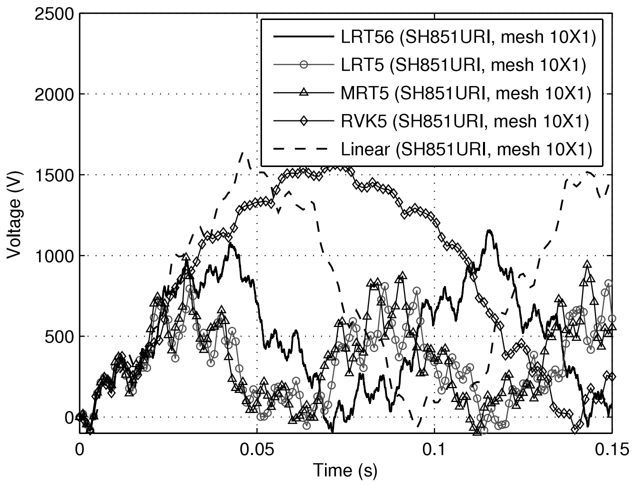

Figure 3. Sensor voltage of the cantilevered beam using various theories.

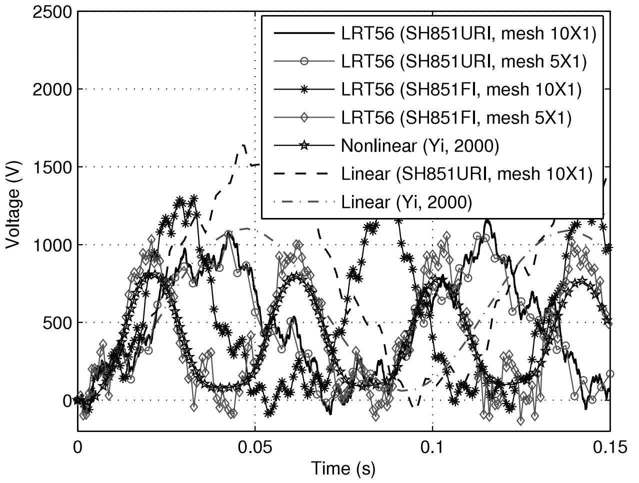

Figure 5. Sensor voltage of the cantilevered beam using LRT56 theory.

SH851FI with two different meshes, which are displayed in figure 4 for the displacement and figure 5 for the sensor output voltage along with a comparison with the literature. From figure 4 it can be seen that the transient response obtained by LRT56 using discretization by 5 × 1 or 10 × 1 SH851URI elements is almost identical. This indicates that the 5 × 1 mesh already yields the converged solution. In figure 4 we have also added a result obtained by a 5 × 1 mesh of SH851FI elements. This was done to compare the results with those given by Yi *et al* [30], who used the fully geometrically nonlinear 3D theory applying a mesh of 5 × 1 20-node solid elements for the master structure and 1 × 1 for the piezoelectric patch without avoiding the locking effects. That is equivalent to using the present mesh of 5 × 1 8-node SH851FI elements. It can be seen that these solutions are indeed in very good agreement. The slight discrepancy of the amplitude of the sensor output voltage signal in figure 5 is explained by different piezoelectric constants d_{31} and d_{32} in [30] as mentioned above. However, due to the locking effects in the models obtained using SH851FI elements, the solutions are not well converged. This is shown by increasing the number of elements from 5 × 1 to 10 × 1 with the same element type SH851FI which leads to a totally different dynamic response compared to the one obtained by 5 × 1 elements.

5.2. *Fully clamped cylindrical shell*

The second example is a fully clamped cylindrical shell with a piezoelectric patch centrally bonded on the top surface as depicted in figure 6. The host structure is made up of orthotropic material, in which the fiber reinforcement is along the Θ^1 direction. The material properties are $E_1 = 124$ GPa, $E_2 = 96.53$ GPa, $\nu_{12} = \nu_{23} = 0.34$, $G_{12} = G_{13} = G_{23} = 6.205$ GPa and $\rho = 1520$ kg m^{-3}. Due to the symmetry, a quarter of the cylindrical shell with a mesh of 8 × 4 SH851URI elements along Θ^1 and Θ^2 axes is used for computation. The Newmark method is applied with a

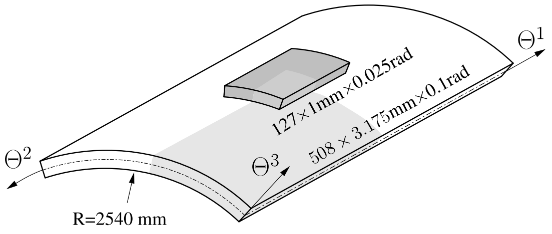

Figure 6. A fully clamped cylindrical shell with centrally bonded piezoelectric.

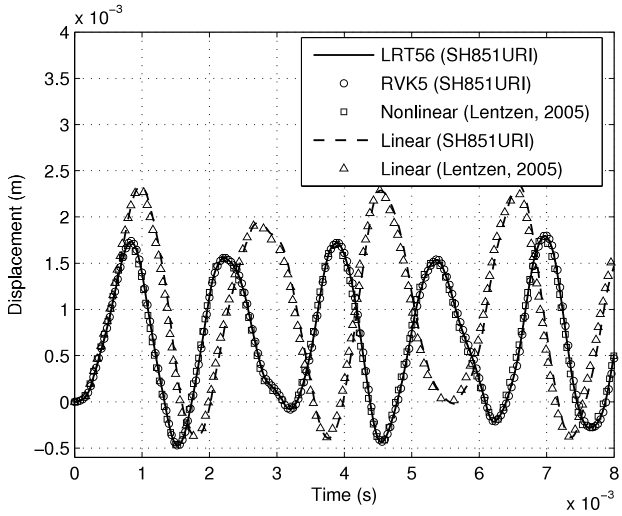

Figure 7. Mid-point displacement of the cylindrical shell under a pressure of 6×10^4 Pa.

time step 1×10^{-5} s for the linear case and 1×10^{-7} s for the nonlinear case. The transient responses of the mid-point displacement and the sensor voltage of the shell structure subjected to a uniformly distributed step load of 6×10^4 Pa are displayed in figures 7 and 8, respectively. It can be seen that there is only a small difference between the results of both displacement and sensor voltage obtained by LRT56 and RVK5 theories, implying that the cylindrical shell undergoes deformations only in the range of moderate rotations. The dynamic response of the mid-point displacement agrees quite well with that in [25] using linear and MRT5 theory in figure 7. Further, increasing the pressure to 6×10^5 Pa, one obtains the dynamic response of displacement and sensor voltage shown in figures 9 and 10, respectively. It can be seen that even at this load only small discrepancies exist between the results predicted by LRT56 and RVK5 theories. This indicates that due to the clamped boundary conditions the cylindrical shell is still undergoing only moderate rotations, although the sensor voltage output would be beyond the range of applicability of the linear piezoelectric constitutive relations in equations (13) and (14).

6. Conclusions and discussions

A large rotation theory, which contains six independent kinematic parameters (expressed by five nodal DOFs) has

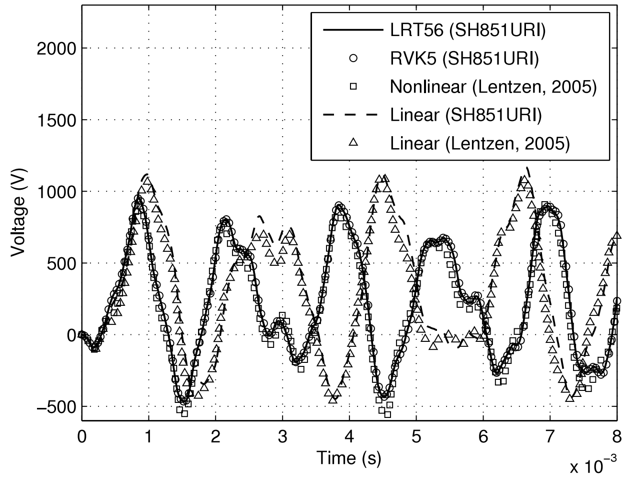

Figure 8. Sensor voltage of the cylindrical shell under a pressure of 6×10^4 Pa.

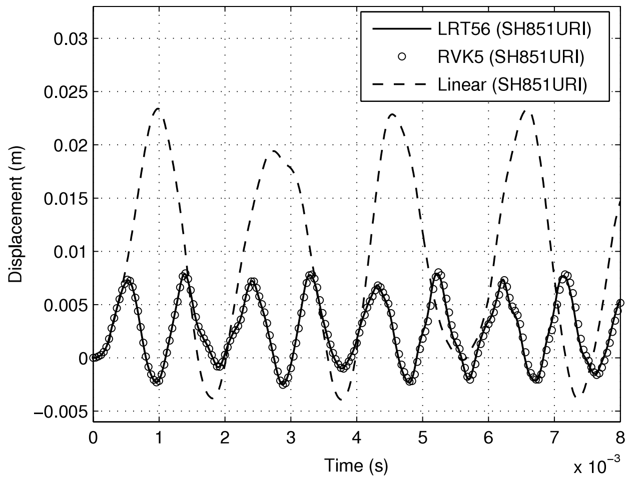

Figure 9. Mid-point displacement of the cylindrical shell under a pressure of 6×10^5 Pa.

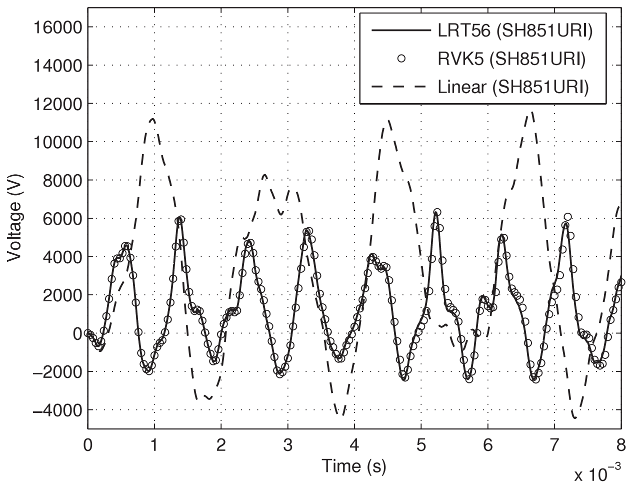

Figure 10. Sensor voltage of the cylindrical shell under a pressure of 6×10^5 Pa.

been developed for FE transient analysis of piezolaminated thin-walled smart structures based on the FOSD hypothesis. The FE dynamic model has been obtained by using eight-node quadrilateral shell elements and linear constitutive equations with the assumption of constant electric field through the thickness of piezoelectric layers. Two integration schemes have been used in the calculations, in which SH851URI stands for the shell element with uniformly reduced integration and SH851FI for full integration. The dynamic equations of both linear and nonlinear cases have been derived by the CDA and the Newmark method. The results obtained by LRT56 theory have been compared with those obtained by simplified nonlinear theories using both SH851FI and SH851URI elements, as well as those presented in the literature. The comparisons illustrate that simplified nonlinear theories can be applied only when structures undergo small or moderate rotations. However, in the case of large rotations occurring in structures, LRT56 has to be considered for dynamic analysis of thin-walled smart structures.

References

[1] Qing X, Kumar A, Zhang C, Gonzalez I F, Guo G and Chang F K 2005 A hybrid piezoelectric/fiber optic diagnostic system for structural health monitoring *Smart Mater. Struct.* **14** S98–103

[2] Sheta E F, Moses R W and Huttsell L J 2006 Active smart material control system for buffet alleviation *J. Sound Vib.* **292** 854–68

[3] Choi S B 2006 Active structural acoustic control of a smart plate featuring piezoelectric actuators *J. Sound Vib.* **294** 421–9

[4] Dube G P, Kapuria S and Dumir P C 1996 Exact piezothermoelastic solution of simply-supported orthotropic flat panel in cylindrical bending *Int. J. Mech. Sci.* **38** 1161–77

[5] Kapuria S and Dube G P 1997 Exact piezothermoelastic solution for simply supported laminated flat panel in cylindrical bending *ZAMM. Z. Angew. Math. Mech.* **77** 281–93

[6] Sze K Y and Yao L Q 2000 A hybrid stress ANS solid-shell element and its generalization for smart structure modeling: part I solid shell element formulation *Int. J. Numer. Methods Eng.* **48** 545–64

[7] Tzou H S and Gadre M 1989 Theoretical analysis of a multi-layered thin shell coupled with piezoelectric shell actuators for distributed vibration controls *J. Sound Vib.* **132** 433–50

[8] Lam K Y, Peng X Q, Liu G R and Reddy J N 1997 A finite-element model for piezoelectric composite laminates *Smart Mater. Struct.* **6** 583–91

[9] Kioua H and Mirza S 2000 Piezoelectric induced bending and twisting of laminated composite shallow shells *Smart Mater. Struct.* **9** 476–84

[10] Wang S Y, Quek S T and Ang K K 2001 Vibration control of smart piezoelectric composite plates *Smart Mater. Struct.* **10** 637–44

[11] Correia V M F, Gomes M A A, Suleman A, Soares C M M and Soares C A M 2000 Modelling and design of adaptive composite structures *Comput. Methods Appl. Mech. Eng.* **185** 325–46

[12] Carrera E and Demasi L 2002 Classical and advanced multilayered plate elements based upon PVD and RMVT. Part 2: numerical implementations *Int. J. Numer. Methods Eng.* **55** 253–91

[13] Alaimo A, Milazzo A and Orlando C 2013 A four-node MITC finite element for magneto-electro-elastic multilayered plates *Comput. Struct.* at press

[14] Panda S and Ray M C 2008 Nonlinear finite element analysis of functionally graded plates integrated with patches of piezoelectric fiber reinforced composite *Finite Elem. Anal. Des.* **44** 493–504

[15] Kapuria S and Dumir P C 2005 Geometrically nonlinear axisymmetric response of thin circular plate under piezoelectric actuation *Commun. Nonlinear Sci. Numer. Simul.* **10** 411–23

[16] Ribeiro P 2008 Non-linear free periodic vibrations of open cylindrical shallow shells *J. Sound Vib.* **313** 224–45

[17] Mukherjee A and Chaudhuri A S 2005 Nonlinear dynamic response of piezolaminated smart beams *Comput. Struct.* **83** 1298–304

[18] Ray M C and Shivakumar J 2009 Active constrained layer damping of geometrically nonlinear transient vibrations of composite plates using piezoelectric fiber-reinforced composite *Thin-Walled Struct.* **47** 178–89

[19] Schmidt R and Vu T D 2009 Nonlinear dynamic FE simulation of smart piezolaminated structures based on first- and third-order transverse shear deformation theory *Adv. Mater. Res.* **79–82** 1313–6

[20] Dash P and Singh B N 2009 Nonlinear free vibration of piezoelectric laminated composite plate *Finite Elem. Anal. Des.* **45** 686–94

[21] Librescu L and Schmidt R 1988 Refined theories of elastic anisotropic shells accounting for small strains and moderate rotations *Int. J. Non-Linear Mech.* **23** 217–29

[22] Schmidt R and Reddy J N 1988 A refined small strain and moderate rotation theory of elastic anisotropic shells *J. Appl. Mech.* **55** 611–7

[23] Palmerio A F, Reddy J N and Schmidt R 1990 On a moderate rotation theory of laminated anisotropic shells—part 1: theory *Int. J. Non-Linear Mech.* **25** 687–700

[24] Kreja I, Schmidt R and Reddy J N 1996 Finite elements based on a first-order shear deformation moderate rotation shell theory with applications to the analysis of composite structures *Int. J. Non-Linear Mech.* **32** 1123–42

[25] Lentzen S and Schmidt R 2005 A geometrically nonlinear finite element for transient analysis of piezolaminated shells *Proc. 5th EUROMECH Nonlinear Dynamics Conf. (Eindhoven, Aug. 2005)*

[26] Lentzen S, Klosowski P and Schmidt R 2007 Geometrically nonlinear finite element simulation of smart piezolaminated plates and shells *Smart Mater. Struct.* **16** 2265–74

[27] Lentzen S 2008 Nonlinear coupled thermopiezoelectric modelling and FE-simulation of smart structures *PhD Thesis* RWTH Aachen University

[28] Chattopadhyay A, Kim H S and Ghoshal A 2004 Non-linear vibration analysis of smart composite structures with discrete delamination using a refined layerwise theory *J. Sound Vib.* **273** 387–407

[29] Ghoshal A, Kim H S, Chattopadhyay A and Prosser W H 2005 Effect of delamination on transient history of smart composite plates *Finite Elem. Anal. Des.* **41** 850–74

[30] Yi S, Ling S F and Ying M 2000 Large deformation finite element analyses of composite structures integrated with piezoelectric sensors and actuators *Finite Elem. Anal. Des.* **35** 1–15

[31] Chróscielewski J, Klosowski P and Schmidt R 1997 Numerical simulation of geometrically nonlinear flexible beam control via piezoelectric layers *Z. Angew. Math. Mech.* **77** (Suppl. 1) S69–70

[32] Chróscielewski J, Klosowski P and Schmidt R 1998 Theory and numerical simulation of nonlinear vibration control of

arches with piezoelectric distributed actuators *Mach. Dyn. Probl.* **20** 73–90
[33] Basar Y, Ding Y and Schultz R 1993 Refined shear-deformation models for composite laminates with finite rotations *Int. J. Solids Struct.* **30** 2611–38
[34] Sansour C and Bednarczyk H 1995 The cosserat surface as a shell model, theory and finite-element formulation *Comput. Methods Appl. Mech. Eng.* **120** 1–32
[35] Kreja I and Schmidt R 2006 Large rotations in first-order shear deformation FE analysis of laminated shells *Int. J. Non-Linear Mech.* **41** 101–23
[36] Habip L M 1965 Theory of elastic shells in the reference state *Ing.-Arch.* **34** 228–37
[37] Kreja I 2007 Geometrically non-linear analysis of layered composite plates and shells *Habilitation Thesis* Politechnika Gdańska